Impact of semi-elliptical cracks on risk assessment for rocket nozzle structural integrity using a fluid-solid interaction

M. Nedjari
Laboratory of Materials and Reactive Systems,
Djillali Liabes University, 22000, Sidi Bel Abbes, Algeria.
e-mail: mohammed.nedjari@univ-sba.dz

B. G. Nasser Muthanna
Department of Mechatronics Engineering, Faculty of Engineering and Computing,
University of Science and Technology, Aden, Yemen.

A. Kirad
Laboratory of Energy Processes and Nanotechnology, University of Blida 1, 09000, Algeria.

C. Ghenai
Sustainable and Renewable Energy Engineering Department, College of Engineering,
University of Sharjah, Sharjah, United Arab Emirates Renewable Energy and Energy Efficiency Research Group,
Sustainable Energy and Power Systems Research Center, Research Institute for Sciences and Engineering,
University of Sharjah, Sharjah, United Arab Emirates.

A. Benarous
Mechanical department, Technology faculty, Saad Dahlab University, Blida, Algeria.

A. Benazza
Laboratory of Materials and Reactive Systems, Djillali Liabes University, 22000, Sidi Bel Abbes, Algeria.

Received 23 October 2024; accepted 23 October 2025

Rocket propulsion systems rely on efficient fluid dynamics within their nozzles to achieve optimal performance. However, rocket nozzles can be susceptible to various failure modes that significantly impact their performances. The aim of this study was to investigate the interaction between fluid flow and rocket nozzle structure to identify critical position prone to failure. It was performed in two steps. In the CFD section, Mach number, static pressure, wall Yplus and axial wall shear stress were predicted. In the FEA section, semi-elliptical cracks were intentionally created at the critical position where the maximum hoop stress was located, provided by the CFD analysis. To comprehensively analyze the nozzle's failure potential, stress intensity factor was numerically carried out and Failure Assessment Diagram (FAD) was employed, as an analytical tool. Each defect depth ratio was evaluated based on its corresponding position within the assessment diagram, while considering factors such as material properties and operating conditions. The main results obtained show that the CFD analysis demonstrated good agreement with the experimental data, with a predicted separation location deviating by only 0.3%. The error between the numerical results and the local measurements on the nozzle wall is 3.84%, which is quite satisfactory. Additionally, the failure assessment indicated that crack depth ratios $(a/t > 0.5)$ in the critical position of the nozzle lead to failure, while ratios $(a/t < 0.5)$ remain within the safe region.

Keywords: Overexpanded nozzle; shock wave; fluid-solid interaction; semi-elliptical crack; failure assessment diagram; risk assessment; FEA.

DOI: https://doi.org/10.31349/RevMexFis.72.020602

1. Introduction

The nozzle is considered one of the most essential components of a rocket as it converts the potential energy into kinetic energy. Additionally, it provides the rocket with thrust, enhancing its performance. Researchers and engineers have developed several designs for this part of the missile to make it more streamlined and to prevent various problems and defects [1, 2]. A rocket engine nozzle commonly operates at high pressures to generate significant thrust, which can potentially lead to wall rupture in the convergent section. Gaining a deeper understanding of the dynamic phenomena occurring within the nozzle area will be crucial for the development of future propulsion systems. This understanding specifically pertains to the unsteady side-loads caused by the interplay between flow separation in the launcher wake and the nozzle structure. The knowledge of these phenomena will play a vital role in advancing the design of upcoming propulsion systems [3-7]. Experiments on rocket nozzles are considered complex and challenging due to the extreme conditions they face during operation, including high temperatures, pressures, and dynamic loads. Additionally, factors such as cost considerations, environmental selection, and other service conditions contribute to the complexity. Furthermore, predicting and preventing nozzle wall rupture and understanding its effects on the rocket engine remain ongoing challenges, and comprehensive literature in this regard is still limited [7-11]. Load determination poses several challenges, such as simulating the intricate interactions among multiple components, addressing diverse loading conditions, and accurately assessing the combined effects of various load types. Finite element analysis (FEA) and computational fluid dynamics (CFD) have become more achievable for conducting failure analysis of structures [12-20]. The concentration of pressure in the critical zones may lead to a damage taking into account the temperatures and geometry of non-uniform structure of rocket nozzle. The crack is one of the principal indicators to detect the state of rocket nozzle through the manner of propagation of crack along the critical zones. In this content, the interaction between internal pressure and rocket nozzle structure was investigated using numerical methods. This technique was used in the pipeline components, gas turbine blade, and rockets [12-15]. Muthanna *et al.* [12] have studied the semi-elliptical cracks in the critical positions of API X52 pipe elbows using fluid-structure interaction (FSI) technique. Moreover, they have proved that this method is more reliable for conducting fracture analysis on gas turbine blades using real operating service conditions [13]. However, the current rocket nozzle analysis was performed in German Aerospace Center (DLR) using dry gaseous nitrogen as flow fluid [21,22]. A comprehensive study on the rocket nozzle using CFD analysis was conducted by Nedjari *et al.* [23]. This work considers a continuation and further advancement for previous work which investigated by Nedjari *et al.* [23]. In the first part of this paper, the fluid interaction of a rocket nozzle was simulated using CFD. The internal pressure distribution obtained from CFD was compared with the experimental measurements conducted by the DLR and showed a good agreement. The CFD analyses were combined and exported into FE software in order to study the fracture phenomenon. Semi-elliptical cracks were created at critical positions on the rocket nozzle based on the maximum value of the hoop stress along the nozzle structure [12,24]. Furthermore, the Stress Intensity Factor (SIF) and Failure Assessment Diagram (FAD) were used to evaluate and predict the integrity and lifetime of the rocket nozzle.

2. Governing equations

The fluid within the computational domain possesses uniform physical properties (molar mass, heat capacities) and is considered non-reactive (gaseous nitrogen, N). The mathematical representation of the conservation principles for mass, momentum, and energy, along with the physical properties of a compressible, 2D axisymmetric, viscous fluid, is formulated as follows:

$$\frac{\partial U}{\partial t}+\frac{\partial F}{\partial x}+\frac{1}{r}\frac{\partial rG(U)}{\partial r}=\frac{S(U)}{r}, \tag{1}$$

where

$$U=\begin{pmatrix}\rho\\ \rho u\\ \rho v\\ \rho E\end{pmatrix},\quad F=\begin{pmatrix}\rho u\\ \rho u^2+p+\tau_{xx}\\ \rho uv+\tau_{xr}\\ (\rho E+p+\sigma_{xx})u+\tau_{rx}v-q_x\end{pmatrix},$$

$$G=\begin{pmatrix}\rho v\\ \rho uv+\tau_{xr}\\ \rho uv^2+p+\sigma_{rr}\\ (\rho E+p+\sigma_{rr})v+\tau_{xr}u-q_r\end{pmatrix},$$

$$\text{and}\quad S=\begin{pmatrix}0\\ 0\\ S_r\\ 0\end{pmatrix}. \tag{2}$$

The stress and heat transfer components are the combined result of both viscous and turbulent contributions. Finally, the source term for the flow is given by

$$S_r=p+\sigma_{\theta\theta}. \tag{3}$$

The pressure is obtained by the equation of state:

$$\frac{p}{\rho}=r_mT, \tag{4}$$

where:

$$r_m=\frac{R}{M_m}. \tag{5}$$

The gas constant is given by:

$$R=C_p-C_v,$$

where C_p and C_v are the specific heats at constant pressure and constant volume, respectively.

The turbulence model chosen for the present study is the Spalart-Allmaras one-equation model, which solves a partial differential equation throughout the entire flow field [25].

The Reynolds stress is given by:

$$\tau_{ij}=2\mu_tS_{ij}, \tag{6}$$

where S_{ij} is the strain-rate tensor, and the eddy viscosity μ_t is given by:

$$\mu_t=\rho\tilde{\nu}\,f_{v1},$$

$$f_{v1}=\frac{\chi^3}{\chi^3+c_{v1}^3},\quad \chi=\frac{\tilde{\nu}}{\nu}.$$

Here, ν is the molecular viscosity, and $\tilde{\nu}$ is the working variable that obeys the transport equation [25].

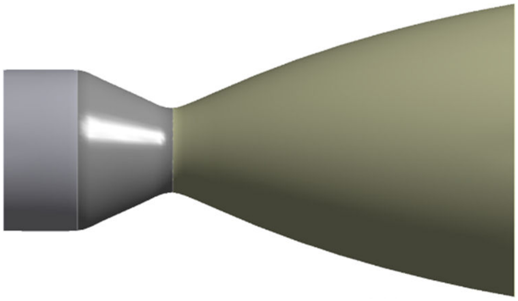

FIGURE 1. Sketch of the rocket nozzle geometry.

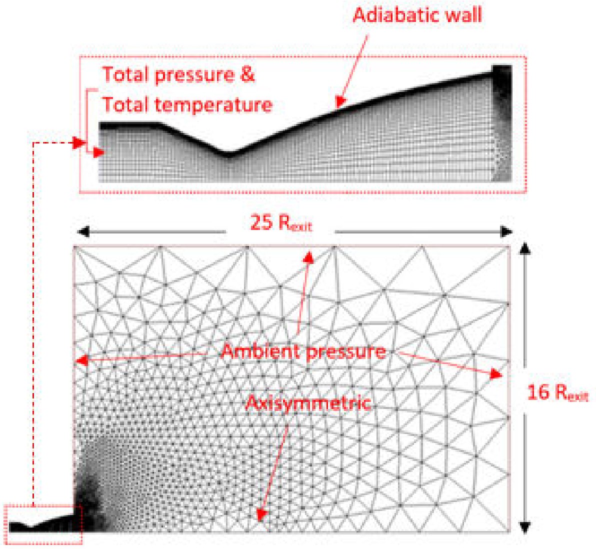

FIGURE 2. Nozzle and computational domain mesh with boundary conditions.

3. Boundary conditions and grid generation

The fluid flow in the internal surface of nozzle has an influence on its structure taking into account the variation of pressure, temperature, velocity and others. Nozzles are regarded as critical pressurized components within the rocket system due to their stress intensification and the impact of irregular sections. However, in this section, the distribution of static pressure is investigated by CFD software. Fig. 1 shows the geometry design of nozzle structure used in this work.

The computational domain in this study was basically depended on the operating conditions which performed on DLR nozzle with real dimensions [21,22]. In a previous CFD study, a free shock separation (FSS) in an over-expanded nozzle was conducted [23]. The fluid used in this study was dry gaseous nitrogen (N_2).

Total pressure and total temperature were introduced in the inlet of nozzle with 25.25 bar and temperatures of 283 K. The nitrogen flow accelerates to supersonic velocities within a convergent-divergent nozzle and exits into the ambient environment, where the pressure and temperature are 1 bar and 270 K, respectively. Based on the experiments, the nozzle walls are assumed to be adiabatic. At the outflow boundaries, all variables, including static pressure, are extrapolated to match the ambient conditions. The nozzle centerline is treated as a symmetry axis. Different mesh with finer grids on nozzle wall were extensively analyzed as indicated in Fig. 2. Figures 3a) and 3b) show the impact of mesh with four different cells (40×103, 90×103, 150×103 and 200×103 cells) on wall shear stress and Mach number. Wall Yplus distribution at the nearest to the wall grid point is illustrated in Fig. 4.

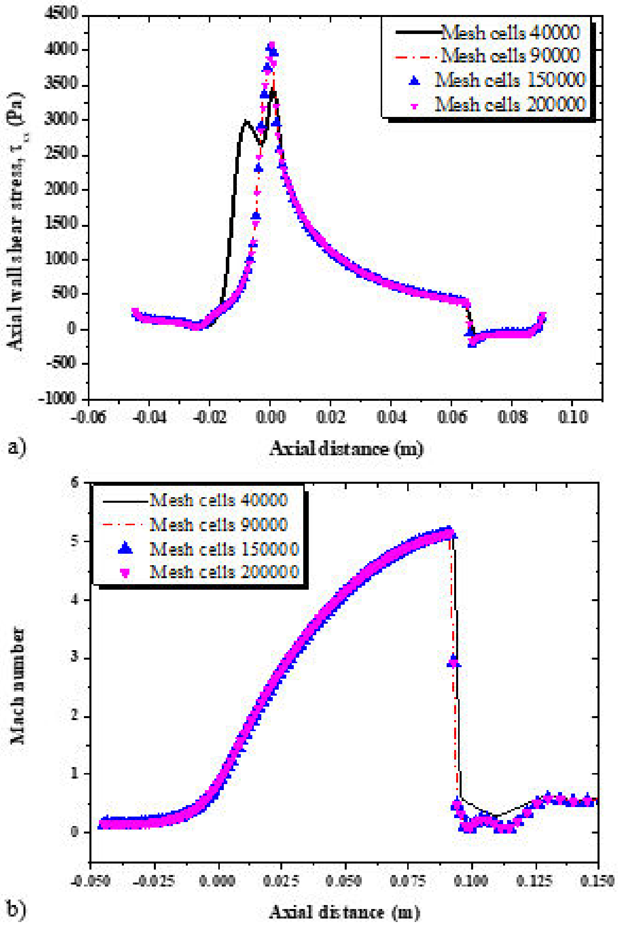

FIGURE 3. Grid refining impact on the nozzle a) wall shear stress, and b) Centreline Mach number.

Figures 3a), 3b) represent the obtained results of wall shear stress and axial Mach number along the nozzle with change of mesh elements (considered as key parameters in detached supersonic compressible flows). It is well observed that the mesh of 45×103 was not the same with the three other meshes. On the other hand, the results of $90 \times 103, 150 \times 103$ and 200×103 are almost identical as exhibited in Fig. 3. In the following work, the mesh with $150,000$ cells was retained to perform CFD analysis.

In CFD analysis, it is a necessary to study y+ parameter in order to assess the quality of the mesh near the nozzle walls. This function is defined as follows:

$$y^+ = \frac{\Delta y}{v}\sqrt{\frac{\tau_\omega}{\rho}}, \tag{7}$$

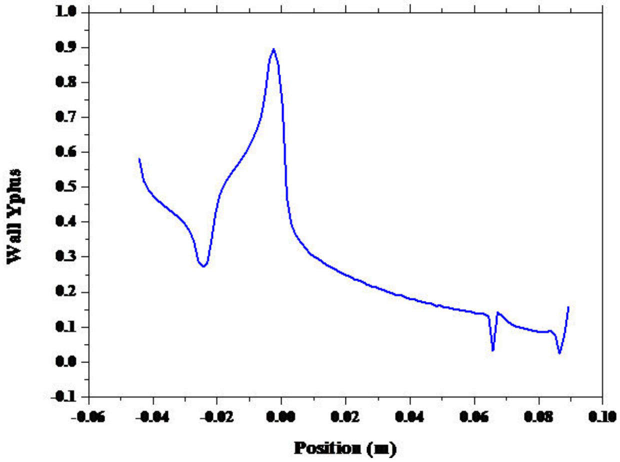

FIGURE 4. Walls $y+$ distribution.

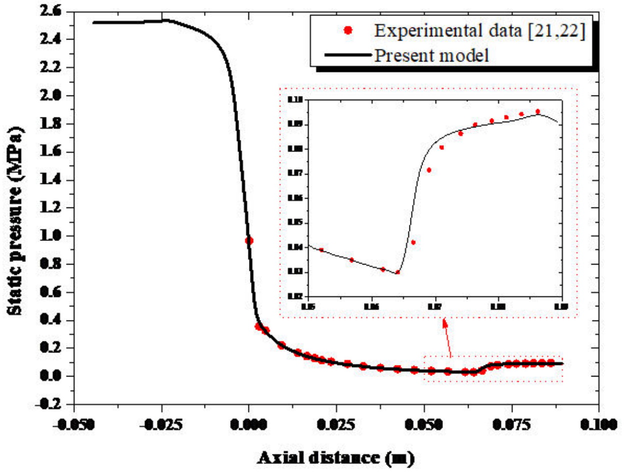

FIGURE 5. Static pressure evolution along the nozzle walls.

where, ρ, v, y, and τ_w are fluid density, flow velocity, distance from the nozzle wall, and wall shear stress of the fluid, respectively. For a turbulent flow, it is desirable to have a Y plus value within $Y+ < 1$, as exhibited by Fig. 4. This represents a good resolution of the turbulent boundary layer and the boundary layer separation in supersonic overexpanded Nozzles [34].

In a rocket nozzle with a convergent-divergent (CD) structure, the static pressure plays a significant role in the performance of the rocket engine. The CD nozzle is designed to accelerate the exhaust gases to supersonic speeds by taking advantage of the expansion of high-pressure gas through the divergent section of the nozzle. Figure 5 shows the results of static pressure distribution along the nozzle obtained by CFD and compared with DLR experiments [21,22]. As indicated in Fig. 5, CFD results almost the same with experiments of DLR data with an average error of 3.84.

Due to irregular sections, the nozzle can be divided into three zones; (i) high pressure, (ii) throat pressure, and (iii) low pressure, as indicated in Fig. 6. Flow separation is characterized by an oblique shock followed by a normal shock

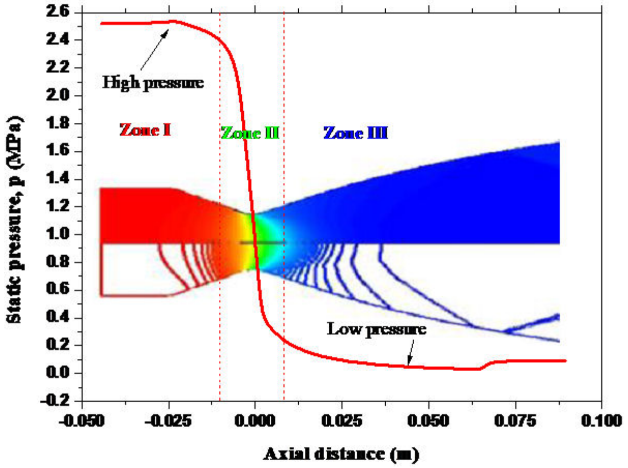

FIGURE 6. General view of static pressure distribution in the internal flow.

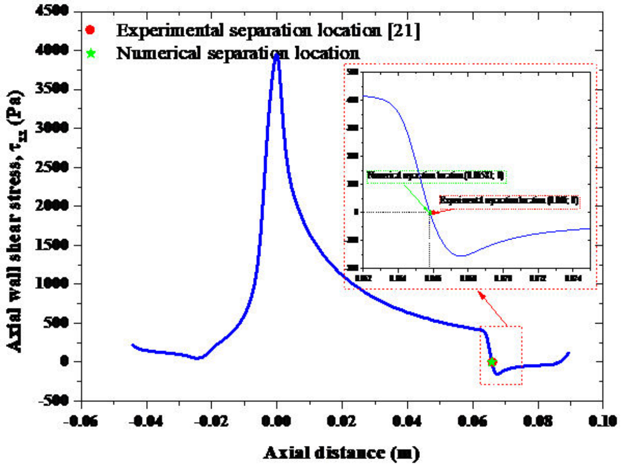

FIGURE 7. Axial wall shear stress vs. axial distance.

near the exit section. A distinct shear region is observed in the post-separation zone, where intense recirculation takes place. The predicted wall static pressure shows a slight recompression upstream of the nozzle exit, which indicates a localized flow separation. This phenomenon can lead to increase the velocity supersonic in CD nozzle. On the other hand, the static pressure and temperature decrease into 1 bar and 270 K respectively as shown in Fig. 5. Therefore, the comparison between the numerical results and the local measurements on the nozzle wall is quite satisfactory, with an error of no more than 3.84%. The error percentage can be calculated using the following expression:

$$\text{Error \%} = \frac{|\text{Experimental value} - \text{Numerical value}|}{\text{Experimental value}} \times 100, \tag{8}$$

in Fig. 7 illustrates the distribution of wall shear stress with axial distance in the nozzle. The separation location was determined based on the wall shear stress obtained by CFD. It was numerically found to be at $X = 0.0658$ m, with an error

TABLE I. Comparison between experiments of DLR data and CFD analysis.

Axial distance	Experimental wall pressure(MPa) [21,22]	Numerical wall pressure (MPa)	Error (%)
0	0.967096463	0.9352	3.298167632
0.00285	0.356904647	0.385	7.871949369
0.0047	0.326203172	0.32016	1.852579135
0.0093	0.222329848	0.2217	0.283294441
0.0139	0.168346421	0.16568	1.583889506
0.0165	0.144296933	0.14836	2.81576845
0.0187	0.13099296	0.12676	3.231440835
0.0207	0.115130531	0.11564	0.442513983
0.0234	0.104896706	0.10201	2.751951326
0.0281	0.088266741	0.082919	6.058613462
0.0326	0.071636775	0.070156	2.067059831
0.0375	0.06140295	0.059856	2.519341497
0.0424	0.051680816	0.050338	2.598287619
0.0472	0.044261293	0.044226	0.079738136
0.052	0.039144381	0.03915	0.014355496
0.0568	0.035050851	0.035033	0.050927808
0.0617	0.031213166	0.031524	0.995841779
0.0641	0.030189784	0.028788	4.643238791
0.0665	0.042214528	0.057001	35.02697418
0.069	0.071636775	0.080008	11.68565307
0.071	0.080847218	0.084778	4.861988602
0.074	0.086475821	0.087887	1.631876667
0.0763	0.09005766	0.089269	0.875727839
0.0789	0.091592734	0.090444	1.254175635
0.0812	0.093127808	0.091214	2.055033348
0.0836	0.094407036	0.09248	2.041199172
0.0862	0.095430418	0.094164	1.327059186

of 0.3% compared to the DLR experiments, $X = 0.066$ [21] as shown in Fig. 7.

4. Nozzle structure and finite element analysis

The distribution of internal pressure (Fig. 7) was imported to the into the nozzle body using structural ANSYS software [26]. However, the rocket nozzle was defined using elastic-plastic behaviour low. The mechanical properties were selected based on the nonlinear true stress-strain behaviour of the steel material used, as shown in Fig. 8. The engineering stress-strain curve was converted to a true stress-strain curve using logarithmic equations [27].

$$\epsilon_t = \int_{L_0}^{L} \frac{1}{L} dl,$$
$$\sigma_t = \frac{P}{A} = \frac{PL}{A_0 L_0} = \sigma_e \frac{L}{L_0} = \sigma_t(\epsilon_e + 1). \tag{9}$$

4.1. Effect of semi-elliptical cracks on the nozzle structure

The rocket nozzle was subjected to an irregular internal pressure as mentioned above. The FSI results are shown in Fig. 9. Obviously, the distribution of pressure around the structure of nozzle effects on the value of stress. Furthermore, the hoop stress distribution is shown in Fig. 9. The maximum hoop stress which indicates by red colour is located in the convergence zone. According to this observation, semi elliptical cracks were supposed to be created in this critical zone [12, 13, 28] in order to study the behaviour of stress intensity factor and failure assessment diagram on nozzle structure with real pressure distribution [21-23].

The rocket nozzle is subjected to various stresses due to its structure and irregular surface. As an essential component of a rocket engine, the nozzle experiences significant mechanical, thermal, and aerodynamic loads during operation. Moreover, the nozzle experiences high-pressure loads

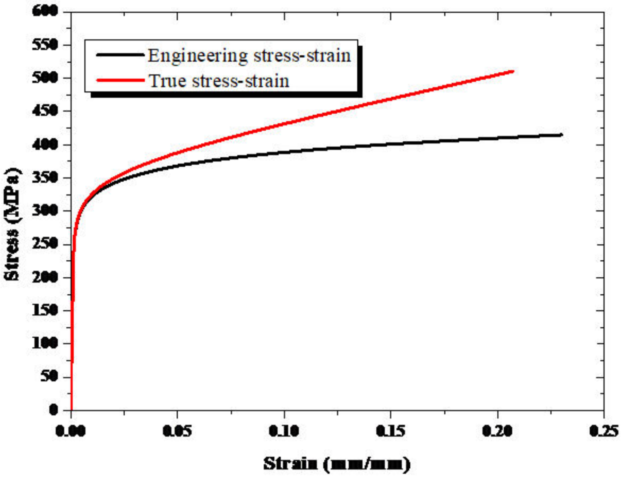

FIGURE 8. Stress strain curve used in the current numerical analysis.

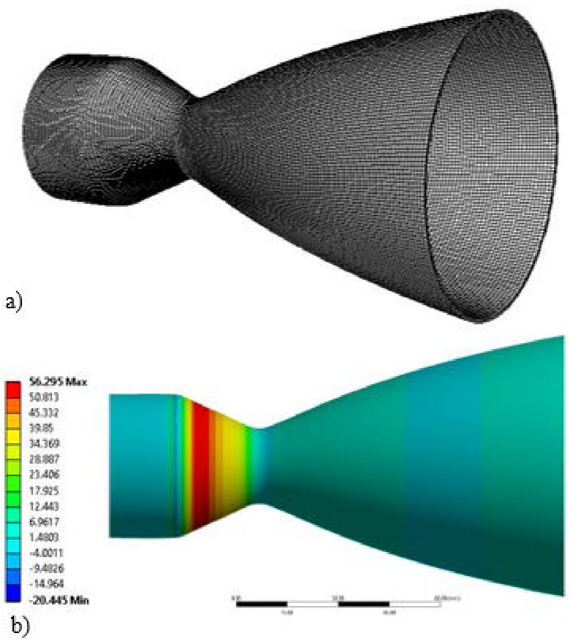

FIGURE 9. a) Mesh, b) hoop stress distribution along nozzle structure using FSI.

due to the combustion gases. As the gases expand and accelerate through the nozzle, they exert significant pressure on the inner surface of the nozzle walls. This pressure can induce stress within the material. Additionally, the irregular surface of the nozzle can result in stress concentrations, where the stress is amplified at specific locations. Irregularities may occur due to manufacturing imperfections, surface defects, or erosion over time. These stress concentrations can weaken the material and potentially lead to structural failure [29-32]. On the other hand, the combustion gases and particles present in the exhaust stream can cause erosion and corrosion on the inner surface of the nozzle. This erosion and corrosion can weaken the material and affect its structural integrity, leading to additional stresses [33].

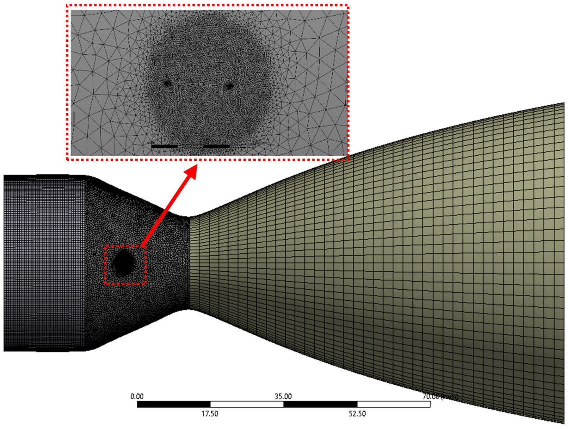

FIGURE 10. Position of the semi-elliptical crack.

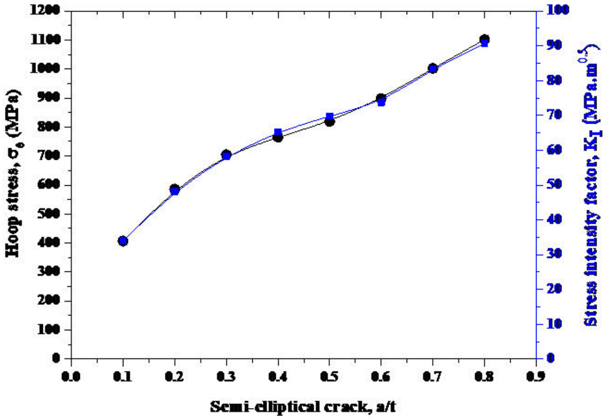

FIGURE 11. Distribution of hoop stress and SIF vs. crack depth ratio a/t.

4.2. Impact of semi-elliptical cracks on hoop stress and stress intensity factor

The stress intensity factor (SIF) is a critical parameter used to assess the severity of stress concentration at the crack tip in a structural component. It is used to assess the criticality of cracks and predict their growth behavior. The specific SIF values for a rocket nozzle would depend on the geometry, material properties, and loading conditions. Stress intensity factor of mode I at any point along the semi-elliptical surface crack can be calculated using the following relation:

$$K_I = \sigma_\theta F \sqrt{2\pi a}, \tag{10}$$

where the parameters σ_θ, F, and a are the hoop stress, the geometry correction factor, and crack depth, respectively. In the current case of a nozzle structure, the SIFs can provide valuable information about the crack propagation tendency. Fig. 11 shows the maximum values of hoop stress and mode I as a function of semi-elliptical crack depth ratios a/t. The relative crack depth ratio (a/t) is defined as the crack depth divided by the nozzle wall thickness. The distribution of mode $I(K_I)$ around the angles of semi-elliptical cracks is shown in Fig. 12.

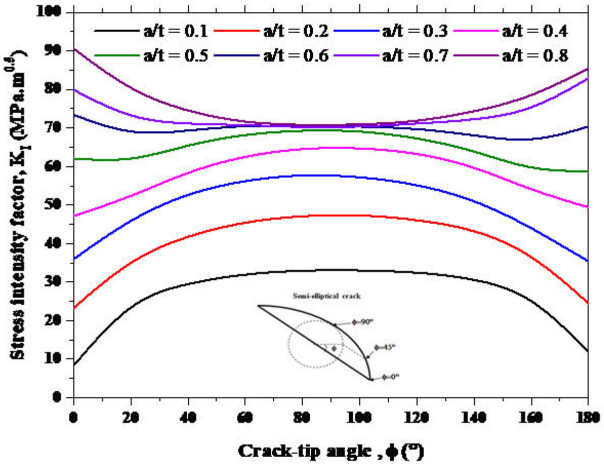

FIGURE 12. Stress intensity factor vs. crack-tip angle.

Hoop stresses and SIFs in mode I generally increase with relative crack depth ratios in rocket nozzles (Fig. 11). When a crack is present, the stress field around the crack tip becomes highly concentrated, leading to increased stress intensity factors. As the relative crack depth ratio increases, the crack becomes deeper in proportion to the thickness of the nozzle wall. The maximum value of K_I is located at the deepest point of the crack front $\phi = 90°$. This means that a larger portion of the wall thickness is affected by the crack, leading to a more significant stress concentration at the crack tip. Consequently, the stress intensity factor in mode I increases with the relative crack depth ratio. The increase in stress intensity factors with higher relative crack depth ratios indicates a higher potential for crack propagation and structural failure. Therefore, it is crucial to carefully assess and monitor crack depths in rocket nozzles to ensure the structural integrity and safety of the system.

4.3. Failure assessment diagram

Failure assessment diagram (FAD) is a tool used to assess the structural integrity and failure risk of a component subjected to a combination of stress and strain. It provides a graphical representation of the combination of stress intensity factor (K) and fracture toughness (Kc) parameters, which helps determine if a crack within a component will propagate or remain stable. The FAD presents three regions; (i) a secure region where the crack is not expected to propagate, (ii) a fail region where rapid crack propagation is likely, and (iii) a safe region between these two regions. On the other hand, in a rocket nozzle, the interaction between high-velocity exhaust gases and the nozzle structure can lead to stresses and deformation. Figure 13 illustrates the FAD for different relative depth ratios $(a/t = 0.1 - 0.8)$. The assessment points for rocket nozzle are located in the plastic collapse zone of the FAD as indicated in Fig. 13. The assessment point $a/t = 0.1$ is almost located at the security region while the points of $a/t = 0.2 - 0.4$ are located in the safety region. However,

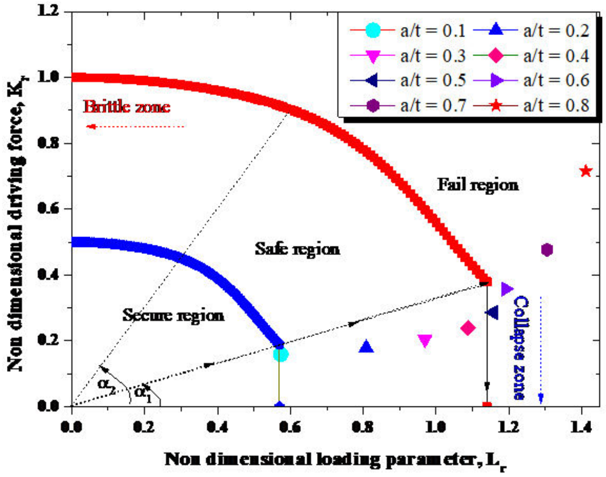

FIGURE 13. Failure assessment diagram for different relative crack depth ratios $(a/t = 0.1 - 0.8)$.

above $50\%(a/t = 0.5 - 0.8)$ of thickness degradation, the rocket nozzle can be placed with the failure region which is considered as a dangerous zone.

5. Conclusions

The fluid flow and failure assessment of the nozzle structure were investigated based on the internal pressure distribution. The pressure distribution obtained from CFD was applied to the FE model. It was noted that the maximum hoop stress occurs in the throat of the convergent nozzle, which can be identified as the critical position. Semi-elliptical cracks with different depth ratios (a/t) were introduced at this critical position. The main conclusions and findings are as follows:

In a rocket nozzle with a convergent-divergent (CD) structure, static pressure plays a critical role in performance. CFD results for static pressure distribution closely match DLR experimental data, demonstrating the effectiveness of the CD nozzle in accelerating exhaust gases to supersonic speeds through pressure expansion.

The nozzle is divided into three zones: high pressure, throat pressure, and low pressure. These pressure variations contribute to the acceleration of exhaust gases and the reduction of static pressure and temperature towards the nozzle's exit.

Wall shear stress distribution was analyzed, and the separation location in the nozzle was determined to be at $X = 0.0658m$, with only a 0.3% error compared to experimental results.

Hoop stresses and stress intensity factors (SIFs) in Mode I increase with the relative crack depth ratio in the nozzle. As cracks deepen, stress concentrations grow, raising the potential for crack propagation and structural failure. Larger crack depths cause more significant stress at the crack tip, highlighting the importance of monitoring crack depths for structural integrity.

The Failure Assessment Diagram (FAD) was used to assess the structural integrity of the nozzle under stress. The FAD identified regions based on crack depth ratios (a/t). Smaller crack depths $(a/t = 0.1 - 0.4)$ are in the safe or secure regions, while crack depths above $50\%(a/t = 0.5 - 0.8)$place the nozzle in the failure region, posing a significant risk of structural failure.

Nomenclature

Symbols

A	Cross-sectional area
C_f	Thrust coefficient
D	Diameter
e	Strain (%)
F	Nozzle thrust
K	Stress intensity factor
K_I	Mode I stress intensity factor (MPa$\cdot$m$^{0.5}$)
K_C	Fracture toughness (MPa$\cdot$m$^{0.5}$)
l	Flatness coefficient
L	Final length (mm)
L_0	Initial length (mm)
L_{cv}	Convergent length
L_{div}	Divergent length
M	Mach number
P	Static pressure
q	Crack-tip angle (°)
R	Radius
r	Radial coordinate
t	Thickness (mm)
T	Static temperature
u_x	Axial velocity
u_r	Radial velocity
X	Axial coordinate
Y^+	Wall Yplus
v	Kinematic viscosity
τ	Viscous stress tensor

Greek Symbols

μ	Dynamic viscosity
ρ	Density
γ	Specific heat ratio

Subscripts

a	Ambient
ch	Chamber
e	Exit
th	Throat
w	Wall

Abbreviations

API	American Petroleum Institute
CFD	Computational Fluid Dynamics
CV	Convergent Nozzle
CV-DV	Convergent-Divergent Nozzle
DLR	German Aerospace Center
DV	Divergent Nozzle

Acknowledgements

The authors would like to acknowledge the financial support of the DGRSDT, the General Direction for Scientific Research and Technological Development, Algeria.

1. D. Mishra, Fundamentals of rocket propulsion (CRC Press, 2017), `https://doi.org/10.1201/9781315175997`
2. P. Sutton George and O. Biblarz, Rocket Propulsion Elements John Wiley and Sons (2016)
3. A. Hadjadj, Y. Perrot, and S. Verma, Numerical study of shock/boundary layer interaction in supersonic overexpanded nozzles, Aerospace science and technology **42** (2015) 158, `https://doi.org/10.1016/j.ast.2015.01.010`
4. V. Lijo *et al.*, Numerical simulation of transient flows in a rocket propulsion nozzle, International Journal of Heat and Fluid Flow **31** (2010) 409, `https://doi.org/10.1016/j.ijheatfluidflow.2009.12.005`
5. L. Garelli, R. R. Paz, and M. A. Storti, Fluid-structure interaction study of the start-up of a rocket engine nozzle, Computers and Fluids **39** (2010) 1208, `https://doi.org/10.1016/j.compfluid.2010.03.005`
6. H. Lüdeke *et al.*, A fluid structure coupling of the ariane-5 during start phase by DES (2008), `https://elib.dlr.de/63201`
7. S. Jack and M. Oschwald, Simulation of Fluid Structure Interaction in Overexpanded Cold Gas Rocket Nozzles Using the DLR TAU Code, In 7th European Conference for Aeronautics and Space Sciences (EUCASS) (2017) `https://elib.dlr.de/116250`
8. E. Martelli *et al.*, Flow dynamics and wall-pressure signatures in a high-Reynolds-number overexpanded nozzle with free shock separation, Journal of Fluid Mechanics **895** (2020) A29, `https://doi.org/10.1017/jfm`
9. M. Bernardini *et al.*, Unsteadiness characterisation of shock wave/turbulent boundary-layer interaction at moderate Reynolds number, Journal of Fluid Mechanics **954** (2023) A43. `https://doi.org/10.1017/jfm.2022.1038`

10. H. Lüddeke, J. B. Calvo, and A. Filimon, Fluid structure interaction at the ariane-5 nozzle section by advanced turbulence models, In ECCOMAS CFD 2006: Proceedings of the European Conference on Computational Fluid Dynamics, Egmond aan Zee, The Netherlands, September 5-8, 2006 (Delft University of Technology; European Community on Computational Methods, 2006). `https://elib.dlr.de/46935`
11. E. Blades, E. Luke, and J. Ruf, Fully coupled fluid-structure interaction simulations of rocket engine side loads, In 48th AIAA/ASME/SAE/ASEE joint propulsion conference and exhibit (2012) p. 3969.
12. B. G. N. Muthanna *et al*., Numerical study of semi-elliptical cracks in the critical position of pipe elbow, Frattura ed Integrità Strutturale **13** (2019) 463, `https://doi.org/10.3221/IGF-ESIS.49.44`
13. A. Mouna *et al*., Corrosion effect, constraint and path orientation estimated in cracked gas turbine blade, Engineering Failure Analysis **110** (2020) 104345, `https://doi.org/10.1016/j.engfailanal.2019.104345`
14. H. Boukortt *et al*., Hydrogen embrittlement effect on the structural integrity of API 5L X52 steel pipeline, International Journal of Hydrogen Energy **43** (2018) 19615, `https://doi.org/10.1016/j.ijhydene.2018.08.149`
15. G. Romano, R. Barretta, and M. Diaco, Solid-fluid interaction: a continuum mechanics assessment, Acta Mechanica **228** (2017) 851, `https://doi.org/10.1007/s00707-016-1738-7`
16. M. Amara *et al*., Effect of sand particles on the Erosioncorrosion for a different locations of carbon steel pipe elbow, Procedia Structural Integrity **13** (2018) 2137, `https://doi.org/10.1016/j.prostr.2018.12.151`
17. Y. Chen *et al*., Theoretical analysis and verification on plastic deformation behavior of rocket nozzle using a novel tube upsetting-bulging method, Materials **16** (2023) 1680, `https://doi.org/10.3390/ma16041680`
18. B. Nigar *et al*., Understanding mechanical failure of graphite rocket nozzle throats under thermal stresses, Aerospace Science and Technology **119** (2021) 107152, `https://doi.org/10.1016/j.ast.2021.107152`
19. C. Fang *et al*., A simplified finite element method for failure analysis in adhesive-bonded nozzle diffuser of solid rocket motors, In Journal of Physics: Conference Series, **2535** (IOP Publishing, 2023) p. 012014, `https://doi.org/10.1088/1742-6596/2535/1/012014`
20. D. Kowollik *et al*., 3D fluid-structure interaction analysis of a typical liquid rocket engine cycle based on a novel viscoplastic damage model, International journal for numerical methods in engineering **94** (2013) 1165, `https://doi.org/10.1002/nme.4488`
21. R. Stark and G. Hagemann, Current status of numerical flow prediction for separated nozzle flows (2007), `https://elib.dlr.de/49262`
22. R. Stark and B. Wagner, Experimental study of boundary layer separation in truncated ideal contour nozzles, Shock Waves **19** (2009) 185, `https://doi.org/10.1007/s00193-008-0174-6`
23. M. Nedjari, A. Benarous, and A. Benazza, Numerical characterization of shock separation in a laboratory-scale nozzle, Revista Mexicana de Física **69** (2023) 010601, `https://doi.org/10.31349/RevMexFis.69.010601`
24. H.-Y. Lai *et al*., Fracture analysis of a piezoelectric elliptical tube subject to internal pressure and thermal loadings, Acta Mechanica **232** (2021) 2493, `https://doi.org/10.1007/s00707-021-02943-4`
25. Č. Kostić, Review of the Spalart-Allmaras turbulence model and its modifications to three-dimensional supersonic configurations, *Scientific Technical Review* **65** (2015) 43, `https://scindeks.ceon.rs/Article.aspx?artid=1820-02061501043K`
26. `https://www.ansys.com/products`
27. A. Petrik and R. Aroch, Usage of true stress-strain curve for FE simulation and the influencing parameters, In IOP Conference Series: *Materials Science and Engineering*, **566** (2019) 012025, `https://doi.org/10.1088/1757-899X/566/1/012025`
28. B. G. N. Muthanna *et al*., Assessment of corroded API 5L X52 pipe elbow using a modified failure assessment diagram, *International journal of pressure vessels and piping* **190** (2021) 104291, `https://doi.org/10.1016/j.ijpvp.2020.104291`
29. W. Choi *et al*., Development of thermal stress concentration factors for life assessment of turbine casings, *International journal of pressure vessels and piping* **98** (2012) 1, `https://doi.org/10.1016/j.ijpvp.2012.07.001`
30. J. Y. Zheng, M. W. Fu, and F. Zeng, Design and development of multi-scaled metallic parts and structures, In Encyclopedia of Materials: Metals and Alloys, pp. 3-18 (Elsevier, 2021), `https://doi.org/10.1016/B978-0-12-819726-4.00137-X`
31. J. Gimeno, O. Venegas, and J. Urbano, Stress Concentration Factor in vessels with circular crosshole: Continuous parameters analysis, *International Journal of Pressure Vessels and Piping* **199** (2022) 104775, `https://doi.org/10.1016/j.ijpvp.2022.104775`
32. R. Molaei *et al*., Fatigue and fracture of additively manufactured metallic materials, *Comprehensive Structural Integrity* (2023) V1, `https://doi.org/10.1016/B978-0-12-822944-6.00010-4`
33. B. G. N. Muthanna *et al*., Inspection of internal erosioncorrosion of elbow pipe in the desalination station, *Engineering Failure Analysis* **102** (2019) 293, `https://doi.org/10.1016/j.engfailanal.2019.04.062`
34. A. Balabel *et al*., Assessment of turbulence modeling for gas flow in two-dimensional convergent-divergent rocket nozzle, *Applied Mathematical Modelling* **35** (2011) 3408, `https://doi.org/10.1016/j.apm.2011.01.013`